Article

Not peer-reviewed version

Adsorption of Hydrogen Sulphide on Activated Carbon Materials Derived from the Solid Fibrous Digestate

Evangelia Choleva , Anastasios Mitsopoulos , Georgia Dimitropoulou , George Em. Romanos , Evangelos P. Kouvelos * , Georgios Pilatos , Stylianos D. Stefanidis , Angelos Lappas , Themistoklis Sfetsas *

Posted Date: 8 June 2023

doi: 10.20944/preprints202306.0589.v1

Keywords: activated carbon; hydrogen sulfide; biogas; physical adsorption; micropores; biogas; solid fibrous digestate; carbon dioxide; mesopores

Article

Adsorption of Hydrogen Sulphide on Activated Carbon Materials Derived from the Solid Fibrous Digestate

Evangelia Choleva [1,2], Anastasios Mitsopoulos [1,4], Georgia Dimitropoulou [1], George Romanos [2], Evangelos Kouvelos [2], George Pilatos [2], Stylianos Stefanidis [3], Angelos Lappas [3] and Themistoklis Sfetsas [1,*]

[1] QLAB Private Company, Research & Development, Quality Control and Testing Services, Thessaloniki, 57008 Greece; t.sfetsas@q-lab.gr
[2] Institute of Nanoscience and Nanotechnology, National Center of Scientific Research "Demokritos", Agia Paraskevi, Athens, 15310, Greece; g.romanos@inn.demokritos.gr, choleva.evangelia@gmail.com
[3] Laboratory of Environmental Fuels/Biofuels and Hydrocarbons, Chemical Process and Energy Resources Institute, CERTH, Thessaloniki, 57001, Greece; angel@cperi.certh.gr
[4] Biogas Lagada SA, 677 Parcel, Kolchiko, Lagadas, 57200, Greece; s.patsatzis@biogaslagada.gr
* Correspondence: t.sfetsas@q-lab.gr; Tel.: +30 2310 784712

Abstract: The goal of this work is to develop a sustainable value chain of carbonaceous adsorbents that can be produced from the solid fibrous digestate (SFD) of biogas plants and further applied in integrated desulphurisation-upgrading (CO_2/CH_4 separation) processes of biogas to yield high purity biomethane. On this purpose, physical and chemical activation of the SFD derived biochar was optimised to afford micro-mesoporous activated carbons (ACs) of high BET surface area (590-2300 m^2g^{-1}) and enhanced pore volume (0.57-1.0 cm^3g^{-1}). Gas breakthrough experiments from fixed bed columns of the obtained ACs, using real biogas mixture as feedstock, unveiled that the physical and chemical activation conclude to different types of ACs which are sufficient for biogas upgrade and biogas desulphurisation respectively. Performing breakthrough experiments at three temperatures close to ambient it was possible to define the optimum conditions for enhanced H_2S/CO_2 separation. It was also concluded that the H_2S adsorption capacity is significantly affected by restriction to gas diffusion. Hence, the best performance was obtained at 50 ^oC and the maximum observed in the H_2S adsorption capacity *vs* the temperature is attributed to the counterbalance between adsorption and diffusion processes.

Keywords: activated carbon; hydrogen sulfide; biogas; physical adsorption; micropores; biogas; solid fibrous digestate; carbon dioxide; mesopores

1. Introduction

Biogas use as a source of renewable energy increases over the years and the demand for economically attractive methods for biogas upgrading are of growing interest. Hydrogen sulfide is one of the main contaminants that needs to be removed before the biogas stream enters the CHP due to its corrosive effect. One of the most effective, low cost and easy to maintain methods for H_2S removal is the in-situ biological reduction, implemented either by adding Iron Salts/Oxides or by air dosing to the digester's slurry where biological anaerobic oxidation of H_2S to elemental sulfur and sulfates happens by Thiobacilus bacteria. Adding Iron Salts/Oxides is a very effective practice in reducing high H_2S levels down to 200–100 ppmv, but fails to maintain stable level of H_2S. Most regularly practiced is the use of liquid $FeCl_2$, while $Fe(OH)_3$, $Fe(OH)_2$ and ferrous chloride $FeCl_3$ can also be involved in their solid form. The method of dosing 3-6% air to biogas ratio can achieve 80–99% H_2S reduction, down to 20–100 ppm H_2S, [1], while the oxygen content will be 0.5-1.8% per vol.. The second most frequently applied process is this of adsorption, which entails trapping of pollutants

 doi:10.20944/preprints202306.0589.v1

on a solid with a high-surface area (activated carbon or crystalline material with high porosity, e.g. zeolites, silica gel, activated alumina), holding the pollutants through physical (weak) attraction forces or *via* chemical bonding. Adsorption is one of the most competitive technologies for precision desulfurization because it is simple and effective (>99%). The most competitive adsorbents for H_2S biogas removal are impregnated activated carbons and iron oxides, [1,2]. Adsorption systems are typically suitable for flow rates between 10–10,000 m^3/h and pollutants concentrations between 0.1–8 g/m^3, [3,4]. Impregnated activated carbons are preferably applied when it is necessary to significantly reduce or eliminate the concentration of H_2S. This is because in addition to the physical adsorption, activated carbons provide catalytic sites for oxidation to elemental sulfur and sulfate thus enhancing the removal capacity of H_2S. The activated carbons (ACs) must maintain a content of 20-30% moisture and the required volume of oxygen. When the levels of H_2S in the feed stream are high (>3000 ppmv), the adsorptive and catalytic sites are saturated making necessary the periodic regeneration of the AC adsorbents. Impregnated products usually exhibit enhanced H_2S removal capacity, from a normal 10–20 kg $H_2S/(m^3$ carbon) for virgin carbon to 120–140 kg $H_2S/(m^3$ carbon). Cons are that the regeneration of the used in the process ACs is not sustainable and consequently the spent carbon must either be landfilled or re-impregnated, adding up to the logistic cost, [5].

There is hereby new interest field emerged of using the Biomass, even better the Solid Fibrous Digestate (SFD) to produce the ACs on-site for the desulfurization of the biogas. This way, a waste product (SFD) is transformed to an effective adsorbent that can be used either on site, thus creating a closed loop value chain within the Biogas plant or implemented to other gas separation and wastewater treatment processes, achieving the effective integration between value chains, [6,7].

Up to date, activated carbon adsorbents for biogas desulphurization have been prepared and studied using the common raw materials usually involved to yield ACs. Guo J. et al [8] prepared chemically and physically activated carbons based on palm and coconut shells and investigated the different mechanisms of H_2S adsorption; physisorption, chemisorption and H_2S oxidation depending on the activation agent, using H_2O, CO_2, KOH and H_2SO_4 and concluded that chemical activation has better dynamic adsorption performances. Longer breakthrough times as well as prolonged exhaustion times seem to increase the H_2S adsorption capacities. Javier P. et al., [9], investigated the production of AC from barley straw via physical activation method with CO_2 and steam and concluded that the optimal conditions for the activation stage with CO_2 were at 800 °C and a residence time of 1 h and at 700 °C and a hold time of 1 h when H_2O is the activating agent, [10–12]. The maximum BET surface area and micropore volume achieved by carbon dioxide activation were of 789 m^2/g and 0.3268 cm^3/g while for steam activation were 552 m^2/g and 0.2304 cm^3/g, representing an increase on both values of more than 42% for the case of activation with carbon dioxide. Those ACs functionalized with CO_2 presented a well-developed micropore structure compared to the lower degree of microporosity endowed in the steam activated carbons. 2, 3, 6 and 9-ring carbon structured adsorbent surfaces have been investigated by Akhtar Hussain [13], using parameters such as the planar and non-planar mode and the surface defects. 6-ring with the vacancy centrally located in non-planar mode illustrated the highest steric heat of sorption (q_{st}) for H_2S while adsorption is performed with significant strength both on non-defected and defected 3-ring model in planar mode. As a general outcome the increase of the size and the structure decreases the q_{st} and the most suitable configuration for the phenomenon to happen is the central, in a non-planar mode. Further to the investigations on the development of highly efficient and selective for H_2S, activated carbon adsorbents, there are also many studies focusing on the engineering part of the desulphurization process, elaborating either standalone processes or cascades that combine different processes such as adsorption on activated carbons and steel wool and absorption into aqueous solutions of amine, sodium hydroxide and calcium hydroxide, [14,15]. The target of these studies is to instigate the overall process with the desired functionality which can be either to enhance the CH_4 content of biogas or to effectively remove H_2S and CO_2. Relevant reported results are presented in Table 1 concluding to the point that combination of calcium hydroxide (1 Molar) and steel wool (Fe and Zn elements) favors CO_2 and H_2S removal (max -44% and -97% respectively) while combination of

Preprints (www.preprints.org) | NOT PEER-REVIEWED | Posted: 8 June 2023 doi:10.20944/preprints202306.0589.v1

sodium hydroxide (1,5 Molar), activated carbon and steel wool favors CH_4% content enhancement (up to +30% max) and CO_2 removal (up to -41% max).

Table 1. Results obtained from cascade processes that combine adsorption and absorption columns for biogas treatment. Absorbers are filled with 1L of solvent while adsorber columns are filled with 500 g of adsorbent, [1].

Gas	Sodium hydroxide(1.5 Molar) + Activated carbon(mass 500 g) + Steel wool(mass 500 g)		Calcium hydroxide(1 Molar) + Steel wool(mass 500 g)	
	P: 2.5 cm of Hg Q: 10 LPM	P: 5 cm of Hg Q: 2 LPM	P: 2.5 cm of Hg Q: 10 LPM	P: 7.5 cm of Hg Q: 2 LPM
CH_4	+12%	+30%	+24%	+28%
CO_2	-55%	-41%	-22%	-44%
H_2S	-97%	-96%	-97%	-97%

Other parameters for optimization related to the process conditions and it was showed that the biogas inlet pressure had varying effects on the performance depending on the composition of the solvent (absorbent) and the type of adsorbent, whereas the amplification of the biogas feed flow rate had a negative effect on the targets of high CH_4 content and effective CO_2 removal, [16–18]. On the contrary H_2S was favored for flow rates up to 10 LPM. While cascades of absorption and adsorption processes offer the flexibility to select amongst a great variety of solvents and adsorbents and to fine tune the conditions towards achieving the required performance, they present also major difficulties related with the need to design and integrate completely different absorber and adsorber columns and the great variety of processes required for the regeneration of solvents and adsorbents along with the different frequency of regeneration. These difficulties are showcased in Table 2.

Table 2. Details of the frequency of regeneration and related data for different reagents, [1].

Name & chemical formula of the reagent	**Cost of the reagent** ($US)	**Concentration of aqueous solution or mass of the adsorbent**	**Volume of biogas purified before saturation** (m^3)	**Cost of chemical for purification** ($US/ m^3)
Monoethanolamine (MEA), **C_2H_7NO**	6.82 per L	10% by volume	165	Regeneration by heating
Sodium hydroxide, **NaOH**	1.36 per kg	1.5 Molar	178	0.46
Granular activated carbon, **AC**	0.2 per kg (limestone)	mass 100 g	117	0.13
Steel wool, **Fe_2O_3**	5.46 per kg	mass 500 g	207	2.64
Calcium hydroxide, **$Ca(OH)_2$**	0.2 per kg	1 Molar	Regeneration up to 5 times	Regeneration by oxidization

Conclusively, the design of cascade processes integrating different solid adsorbents with tailor made gas adsorption and separation capacity seems to be a more feasible solution for applications in biogas desulphurization and upgrading.

In this context, the present study achieves the dual target of developing effective adsorbents from the waste effluent of a biogas plant and further endowing them with enhanced CO_2 separating or H_2S

Preprints (www.preprints.org) | NOT PEER-REVIEWED | Posted: 8 June 2023 doi:10.20944/preprints202306.0589.v1

separating capacity. Hence, the developed, in this work, activated carbons can be applied in stand-alone or cascade processes with the targets of desulphurising biogas and enhancing its CH_4 content. Starting from the solid fraction of digestate, pre-treatment and pyrolysis techniques are firstly optimized to achieve high yields of biochar, [19–22]. Further, biochar is converted to activated carbon by applying a variety of physical and chemical activation methods with CO_2, H_2O and KOH. Breakthrough experiments in fixed bed columns at different temperatures using real biogas mixtures are performed and the obtained gas uptake and separation performances of the various ACs are scrutinized against their pore structural and surface chemistry properties. Conclusively, the outcome of this work is an optimized workflow that starts from SFD and ends up with a tailor-made adsorbent for either enhanced CO_2 or H_2S separation.

2. Experimental Procedures

2.1. Materials and Methods

The SFD (solid fibrous digestate) is obtained from the whole digestate (WD) of the anaerobic digester of a biogas plant, after separation in a screw filter press separator, followed by drying. The total solids (TS) content of the SFD is between 25 to 30%. In order to free the SFD precursor materials from their inorganic content, wash steps with HNO_3 1% solution were added. The resulting washed material are further abbreviated as SFD-W.

2.2. Equipment and procedure of SFD pyrolysis and biochar activation

The carbonization of the SFD and SFD-W was carried out via slow pyrolysis in a bench-scale fixed bed reactor [Figure 1], investigating the temperature parameter along with the residence time of the pyrolysis. A sample size of 5 g was carbonized at different temperatures (600-800 °C) and duration (30-120 min) [Table 3]. Achieving a higher pyrolysis yield was of high priority in this study since the overall yield, of the whole process is relatively low. Thus, as long as the surface and pore characteristics are good, the pyrolysis parameters that favor the biochar yield are preferred.

Table 3. Biochar yield (%wt., dry matter feed) at various pyrolysis temperatures and times.

Pyrolysis Temperature	Pyrolysis Time	Biochar Yield (%wt., Dry Matter feed)	
(°C)	(min)	**BC-SFD**	**BC-SFD-washed**
600	30	35.90	28.3
600	60	35.30	28.4
600	120	34.50	27.4
700	30	34.10	26.8
700	60	34.00	26.6
700	120	32.70	26.5
800	30	32.70	25.0
800	60	32.80	24.8
800	120	32.10	24.5

Biochar materials derived from the carbonization of the untreated SFD (BC-SFD) had higher ash content (more than 33,60%) while the pretreated BC-SFD-W materials had less than half ash content (up to 18,10%), [see also Tables 7, 8]. This indicates that the removal of part of the inorganic compounds (~72%) from the precursor material with the HNO_3 pretreatment is a highly important stage that must be common to any type of activated carbon development as it allows the carbonization process to expand the carbon matrix.

Preprints (www.preprints.org) | NOT PEER-REVIEWED | Posted: 8 June 2023 doi:10.20944/preprints202306.0589.v1

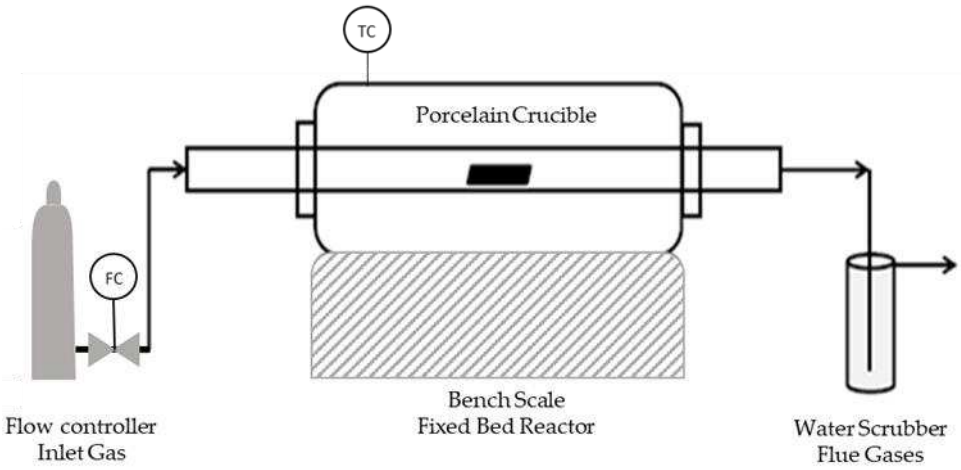

Figure 1. Pyrolysis Reactor.

The biochar activation was carried out *via* slow pyrolysis in a bench-scale fixed bed reactor. Physical activation was carried out (a) with H_2O (1 mL/min) at different temperatures (700-900 °C) and activation duration (15-90 min) (Table 4), with the water vapor flow controlled via a Bronkhorst CEM-System (Controlled Evaporation and Mixing); (b) with CO_2 (50mL/min) at 850°C and activation duration of 150 min. For the chemical activation with KOH, biochar was mixed with solutions of KOH of different concentrations to achieve KOH/biochar ratios of 1:4 (Table 5). After evaporation of the H_2O, the mixture was activated at 600-800 °C for 30-120 min.

Table 4. Activated carbon yield (%wt., dry matter feed), with physical activation (H_2O) at various activation temperatures, steam flow and activation time.

Activation Temperature (°C)	**Steam flow** (mL/min)	**Activation Time** (min)	**Activated Carbon Yield** (%wt., Dry Matter feed) **AC-H_2O**
700	1	30	74.7
700	1	60	65.0
700	1	90	57.1
800	1	30	42.7
800	1	45	35.8
800	1	60	31.5
900	1	15	47.2
900	1	30	33.0
900	1	45	23.3

Table 5. Activated carbon yield (%wt., dry matter feed), with chemical activation (KOH) at various activation temperatures, reagent KOH to biochar ratio and activation time.

Activation Temperature (°C)	Ratio KOH/BC	Activation Time (min)	**Activated Carbon Yield** (%wt., Dry Matter feed) AC-KOH
600	4	30	76.3
700	4	30	73.7
800	1	30	69.2
800	2	30	66.3
800	4	30	66.1
800	4	60	49.0
800	4	120	62.6

Preprints (www.preprints.org) | NOT PEER-REVIEWED | Posted: 8 June 2023 doi:10.20944/preprints202306.0589.v1

2.3. Test rig for Biogas breakthrough experiments

The experimental system for obtaining the breakthrough curves consists of 3 parts; the inlet gas manifold, the fixed bed adsorber and a gas detection system. There are 2 bottles with gases, one with Nitrogen and one with the synthetic biogas (57%CH_4, 42%CO_2, 0,5%O_2 and 500ppm H_2S). The inlet gas flow rates are controlled by a mass flow controller (MFC) and a three-way valve which is installed upstream the MFC to allow the selection of either Nitrogen or Biogas mixture. The adsorber is a horizontal stainless steel tubular fixed bed 7.9cm long and of 4.8mm inner diameter. To initiate the experimental procedure the activated carbon sample is positioned inside the adsorber tube which is wall-heated by a heating mantle powered by a Variac Variable AC transformer. A temperature sensor is used to observe the temperature. Before each breakthrough experiment, the samples were regenerated under nitrogen stream and temperature of 250°C. After lowering the temperature to the experimental value, the inlet stream is switched to by-pass and the nitrogen gas is then switched to the biogas stream. As soon as the concentration of the H_2S is stabilized to the expected level (500ppm) the inlet biogas stream is switched and allowed to pass through the adsorber containing the activated carbon sample. Thus, the adsorption phenomena happen and the breakthrough curves of H_2S and CO_2 can be logged via the software of the respective gas sensors. The concentrations of H_2S and CO_2 in the biogas stream escaping the adsorber column were quantitavely monitored using SGX ECVW EK3 Electochemical and Pellistor Gas Sensor Evaluation Kit and Rapidox Logger 7100 multigas analyzer respectively. The experiments were conducted at adsorption temperature of 25-70°C and the inlet gas flow was set to 50mL/min. Measuring the real flow of the outlet biogas mixture downstream the adsorber and taking into account the dimensional characteristics of the tubular reactor and the consistency of the synthetic biogas mixture the pressure inside the reactor has been calculated at an average of 0,044 millibar and the overflow rate at 220 cm/min (3.66 cm/sec) on average. The adsorption temperature affects the kinematic viscosities of the gases in the mixture, thus the flow characteristics vary, although slightly, for every single experiment, [Table 6].

Table 6. Experimental conditions of the biogas breakthrough tests.

Activated carbon	Reactor temperature (°C)	Flow characteristics					
		Q_{biogas} (mL/min)	ΔP_{biogas} (millibar)	Density (g/cm³)	$V_{average}$ (cm/min)	η_{biogas} (poise)	h (mm)
AC-H_2O	25	39.75	0.0401	0.0423	219.78	9.97E-06	1034.54
	50	40.03	0.0447	0.0445	221.33	1.10E-05	975.78
	70	39.10	0.0472	0.0449	216.18	1.19E-05	934.02
AC-KOH	25	39.77	0.0401	0.0423	219.89	9.97E-06	1034.54
	50	39.85	0.0445	0.0443	220.33	1.10E-05	975.78
	70	39.73	0.0480	0.0457	219.67	1.19E-05	934.02
AC-CO_2	25	40.12	0.0404	0.0426	221.82	9.97E-06	1034.54
	50	40.05	0.0447	0.0445	221.44	1.10E-05	975.78
	70	39.02	0.0471	0.0448	215.74	1.19E-05	934.02

Preprints (www.preprints.org) | NOT PEER-REVIEWED | Posted: 8 June 2023 doi:10.20944/preprints202306.0589.v1

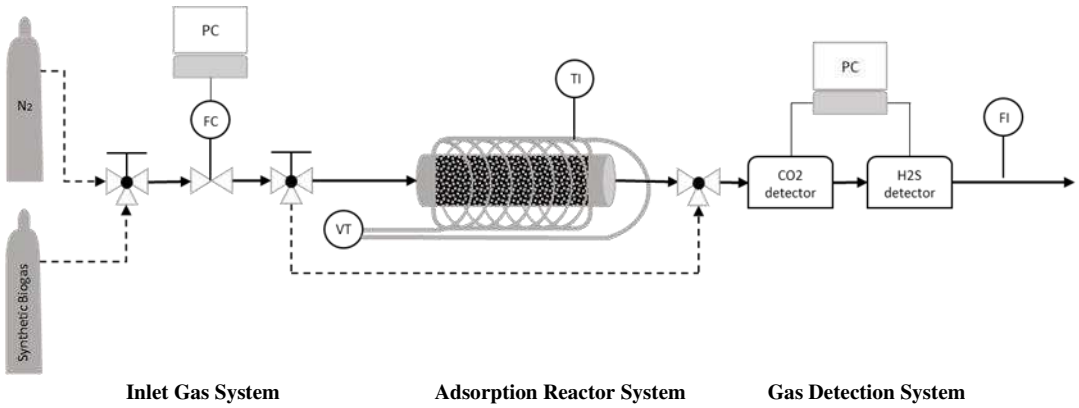

Figure 2. Adsorption Reactor; FC: Flow Controller, VT: Variac Transformer, TI: Temperature Indicator, FI: Flow Indicator.

3. Results and discussion

3.1. Biochar yield

The biochar yield of both untreated solid fibrous digestate and the pretreated with 1% HNO_3 is displayed in Table 3. The results imply that pyrolysis at 600°C achieves the highest yield compared to higher temperatures, while residence pyrolysis time seems to not affect the biochar yield. It should be noticed however that shorter duration of pyrolysis has given the optimal yield of biochar, e.g., 30 and 60 mins for the biochar produced from the non-washed SFD and the one washed with 1% HNO_3 solution prior to the pyrolysis respectively, [Table 3]. Since decreased pyrolysis temperature and shorter carbonization time favors biochar yield, the final preferred product is named BC-600°C-30min-SFD-W, which stands for Biochar produced from Pyrolysis at 600°C for 30mins using as a precursor material the Solid Fibrous Digestate from Biogas Lagada SA plant, pretreated in prior with 1% HNO_3 solution.

3.2. Elemental analysis results and ash content of biochar

Elemental analysis showed that the Carbon content is increased in the biochar compared to its precursor material, [Table 7, 8]. Increasing the pyrolysis temperature, the carbon content of the biochar is increased while decreasing its hydrogen content, [Table 7, 8]. Likewise, though happens when extending the residence time of the pyrolysis. At low temperatures up to 200°C the amount of hydrogen drops due to decrease of the moisture content in the biochar which is also indicated by the reduction of the oxygen content. Up to 600 °C hydrogen content drops rapidly in the step of framework formation, presumably due to the completion of alkyl fragmentation. At higher temperatures up to 800 °C the nitrogen content drops and the same holds for hydrogen content. The ongoing lowering of the amount of nitrogen shows that further densification occurs that mainly involves elimination of nitrogen-containing side products. Furthermore, the processes occurring at 800 °C can be described as an on-going condensation of the aromatic systems upon further elimination of elemental hydrogen and nitrogen.

Table 7. Ash content and elemental analysis of biochar materials derived from the untreated SFD.

Pyrolysis Temperature (°C)	Pyrolysis Time (min)	Ash	C	H	N	O	H/C	O/C
			(%wt., Dry Matter feed)					
600	30	35.30	58.80	1.60	0.50	3.70	0.33	0.05
600	60	33.90	58.60	1.60	0.80	5.10	0.32	0.07
600	120	33.60	61.40	1.30	0.90	2.80	0.25	0.03
700	30	38.20	58.70	1.10	0.50	1.40	0.23	0.02

Preprints (www.preprints.org) | NOT PEER-REVIEWED | Posted: 8 June 2023 doi:10.20944/preprints202306.0589.v1

700	60	38.00	58.90	1.30	0.70	1.20	0.27	0.02
700	120	37.60	60.90	0.90	0.70	0.00	0.18	0.00
800	30	39.10	61.10	0.70	0.30	0.00	0.14	0.00
800	60	37.00	61.20	0.60	0.50	0.70	0.12	0.01
800	120	38.30	60.30	0.40	0.90	0.10	0.07	0.00

Table 8. Ash content and elemental analysis of biochar materials derived from the pre-treated SFD.

Pyrolysis Temperature (°C)	Pyrolysis Time (min)	**Ash**	**C**	**H**	**N**	**O**	**H/C**	**O/C**
		(%wt., Dry Matter feed)						
600	30	14.20	77.70	2.20	0.60	5.10	0.35	0.05
600	60	16.80	76.20	1.90	1.30	3.80	0.31	0.04
600	120	14.60	80.60	1.70	0.00	3.10	0.25	0.03
700	30	16.80	77.20	1.80	1.20	3.00	0.28	0.03
700	60	17.80	77.70	1.50	1.10	1.80	0.24	0.02
700	120	15.70	78.30	1.60	1.00	3.50	0.24	0.03
800	30	16.30	86.80	0.70	1.40	0.00	0.09	0.00
800	60	17.70	78.80	0.90	0.00	2.50	0.14	0.02
800	120	18.10	82.30	0.60	0.90	0.00	0.09	0.00

3.3. Pore structural characteristics of the developed biochars and activated carbons.

The surface and pore structural properties of the resulting biochars and activated carbons were determined by N_2 sorption-desorption at -196 °C using the Autosorb-1 MP (Kr-upgrade) gas sorption analyzer of Quantachrome. Before each measurement, all samples were outgassed at high vacuum and a temperature of 250°C for 24 hours. As indicated from the results included in Tables 9 and 10, biochars produced from SFD previously being washed with HNO_3 1% have higher BET (in the range of 300-350 m^2/g) than those produced from not washed SFD (<50 m^2/g). Washing the SFD with HNO_3 1% can increase the BET by at least 7 times (and up to 19 times) and the Total Pore Volume by at least 3 times (and up to 7 times), respectively. Pyrolysis temperature and residence time affect the material's surface and pore characteristics; higher pyrolysis temperature causes higher BET and Total pore volume while longer pyrolysis residence time seems to not affect significantly the porosity and the surface characteristics. Biochars obtained by SFD-W were transformed into activated carbon using physical activation with H_2O [Table 4] and CO_2 [50 mL/min at 850 °C and activation duration of 150 min] and chemical activation with KOH [Table 5]. In Figure 3 we present the N_2 (77K) adsorption/desorption isotherms and the respective pore size distribution of three selected samples, AC-H_2O, AC-KOH, and AC-CO_2). AC-H_2O was produced with H_2O activation for 60 minutes at 800 °C and a water vapor flow rate of 1 mL/min. Sample AC-KOH was produced *via* 30 minutes chemical activation at a KOH molar ratio of 4:1 and temperature of 800 °C, while AC-CO_2 was produced by physical activation at 850 °C for 150 minutes under a constant CO_2 flow rate of 50 mL/min. The pore size distributions were derived with the QSDFT method for carbon and cylindrical pores, which was applied on both the adsorption and desorption branches of the isotherm. The micropore and external surfaces presented in Tables 9, 10 and 11 were derived from the analysis of the corresponding α_s-plots using the N_2 (77K) adsorption isotherm of a non-porous carbon as the reference one. From the shape of the adsorption isotherms and the respective pore size distributions it is concluded that physical activation of SFD derived biochar yields activated carbons with extended mesopore structure. These carbons have actually a bimodal pore size distribution comprising micropores of the order of 12 Å and mesopores of the order of 50 Å. On the contrary chemical activation with KOH leads to an almost purely microporous material with astonishing high surface area (2272 m^2/g) and enhanced micropore volume of about 0.9 ml/g.

Preprints (www.preprints.org) | NOT PEER-REVIEWED | Posted: 8 June 2023 doi:10.20944/preprints202306.0589.v1

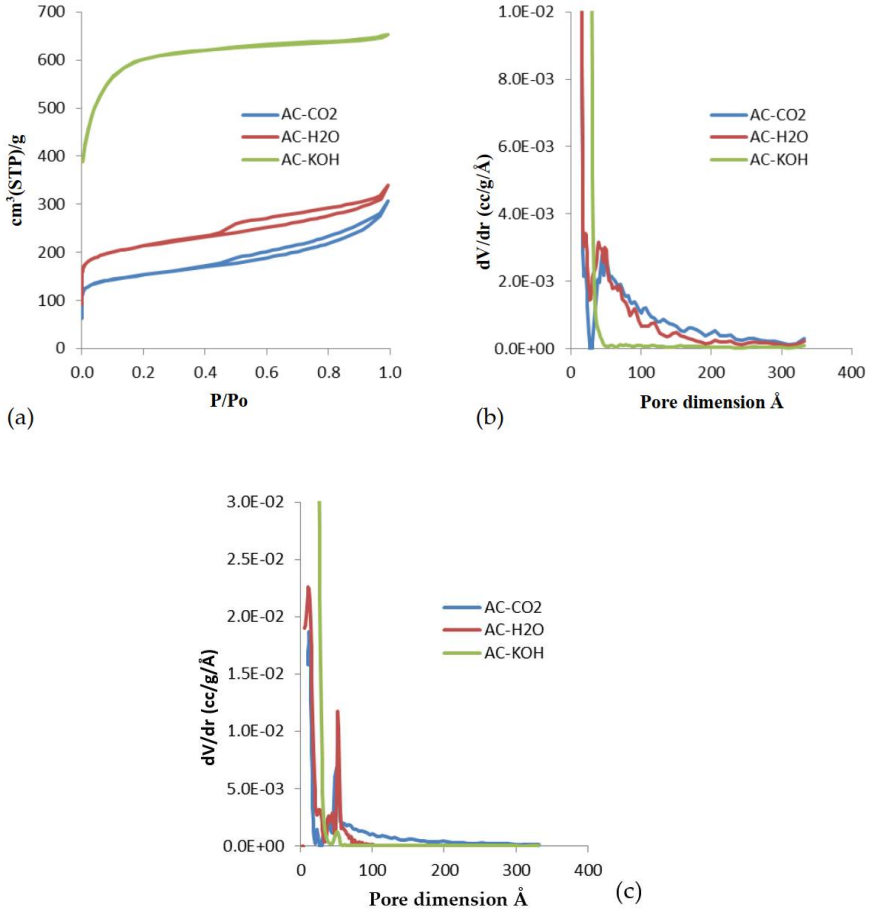

Figure 3. (a) N_2 (77K) adsorption isotherms of porous carbons activated with various methods of physical and chemical activation. **(b)** QSDFT derived pore size distributions obtained from the adsorption branch of the isotherms. **(c)** QSDFT derived pore size distributions obtained from the desorption branch of the isotherms.

Table 9. Surface characteristics and porosity of biochar materials derived from the untreated SFD.

Pyrolysis Temperature (°C)	Pyrolysis Time (min)	BET (m^2/g)	Micropore surface (m^2/g)	External surface (m^2/g)	Micropore Volume (cm^3/g)	Total pore Volume (cm^3/g)
600	30	18	10	8	0.004	0.021
600	60	17	11	6	0.004	0.019
600	120	15	7	8	0.003	0.020
700	30	43	28	15	0.011	0.040
700	60	35	25	10	0.010	0.035
700	120	27	16	12	0.006	0.034
800	30	38	18	20	0.007	0.043
800	60	43	22	21	0.009	0.056
800	120	38	20	18	0.008	0.055

Preprints (www.preprints.org) | NOT PEER-REVIEWED | Posted: 8 June 2023 doi:10.20944/preprints202306.0589.v1

Table 10. Surface characteristics and porosity of biochar materials derived from the pretreated SFD.

Pyrolysis Temperature (°C)	Pyrolysis Time (min)	BET (m^2/g)	Micropore surface (m^2/g)	External surface (m^2/g)	Micropore Volume (cm^3/g)	Total pore Volume (cm^3/g)
600	30	279	263	16	0.103	0.125
600	60	276	265	13	0.103	0.129
600	120	287	268	20	0.104	0.135
700	30	291	279	12	0.108	0.127
700	60	275	263	12	0.102	0.122
700	120	288	278	10	0.107	0.125
800	30	363	339	24	0.132	0.165
800	60	313	298	15	0.115	0.138
800	120	317	292	25	0.113	0.151

Table 11. Surface characteristics and porosity of activated carbons AC-H_2O, AC-KOH and AC-CO_2 produced by activation of biochar which has been derived from the pretreated SFD.

Sample	Means of activation	BET (m^2/g)	Micropore surface (m^2/g)	External surface (m^2/g)	Micropore Volume (cm^3/g)	Total pore Volume (cm^3/g)
AC-H_2O	H_2O	790	644	146	0.31	0.53
AC-CO_2	CO_2	568	355	213	0.224	0.48
AC-KOH	KOH	2272	2174	98	0.89	1.011

3.3. Surface chemistry of activated carbons.

Apart from the pore structural characteristics, the surface chemistry of the activated carbons may have a significant effect on their gas adsorption capacity. Especially the selectivity of CO_2 over CH_4 and of H_2S over CO_2 can be defined by the specific interactions of the gases with the functional groups sprawled on the pore surface of the AC samples. Hence, ATR-FTIR analysis was conducted with an Attenuated Total Reflectance (Brucker FTTR Spectrometer Alpha II, which features a monolithic diamond crystal), to detect and determine the several oxygenated functional groups that usually exist on the surface of ACs. The results presented in Figure 4 show that the physical activation methods, apart from being technically easy and sustainable, do not affect gravely the chemical composition of the formed carbons.

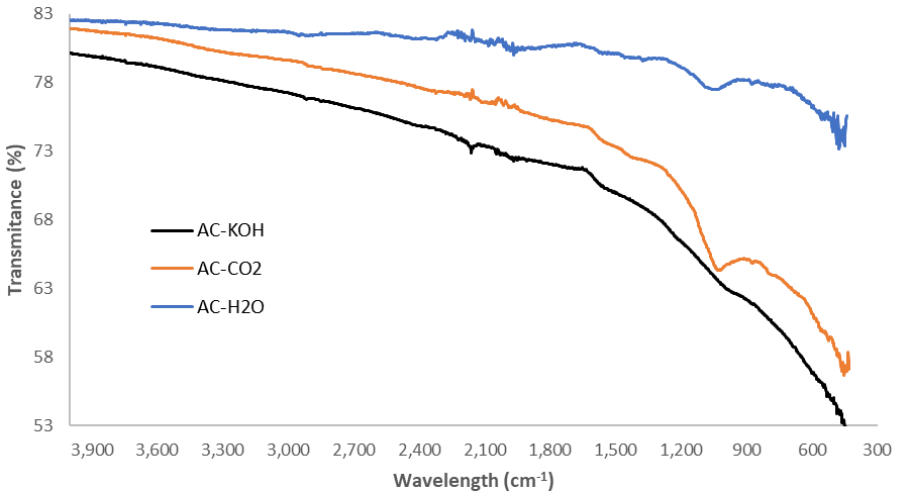

Figure 4. FTIR spectra of the chemically and physically activated carbons.

Preprints (www.preprints.org) | NOT PEER-REVIEWED | Posted: 8 June 2023 doi:10.20944/preprints202306.0589.v1

The peaks corresponding to C-O and C=O stretching vibrations are clearly distinguished in the AC-H_2O and AC-CO_2 samples whereas they are eliminated in the AC-KOH sample. This is an important result that will be discussed in the following section in conjunction with the pore structural features of the AC samples and their capacity to selectively adsorb CO_2 or H_2S.

3.4. Biogas breakthrough curves. Gas separation performance of the developed ACs

Figure 5 depicts the H_2S and CO_2 breakthrough curves obtained from samples AC-H_2O, AC-CO_2 and AC-KOH under the conditions described in Section 2.3 (Table 6). Having interpreted the breakthrough curves, the complete set of results is presented in Tables 12–16.

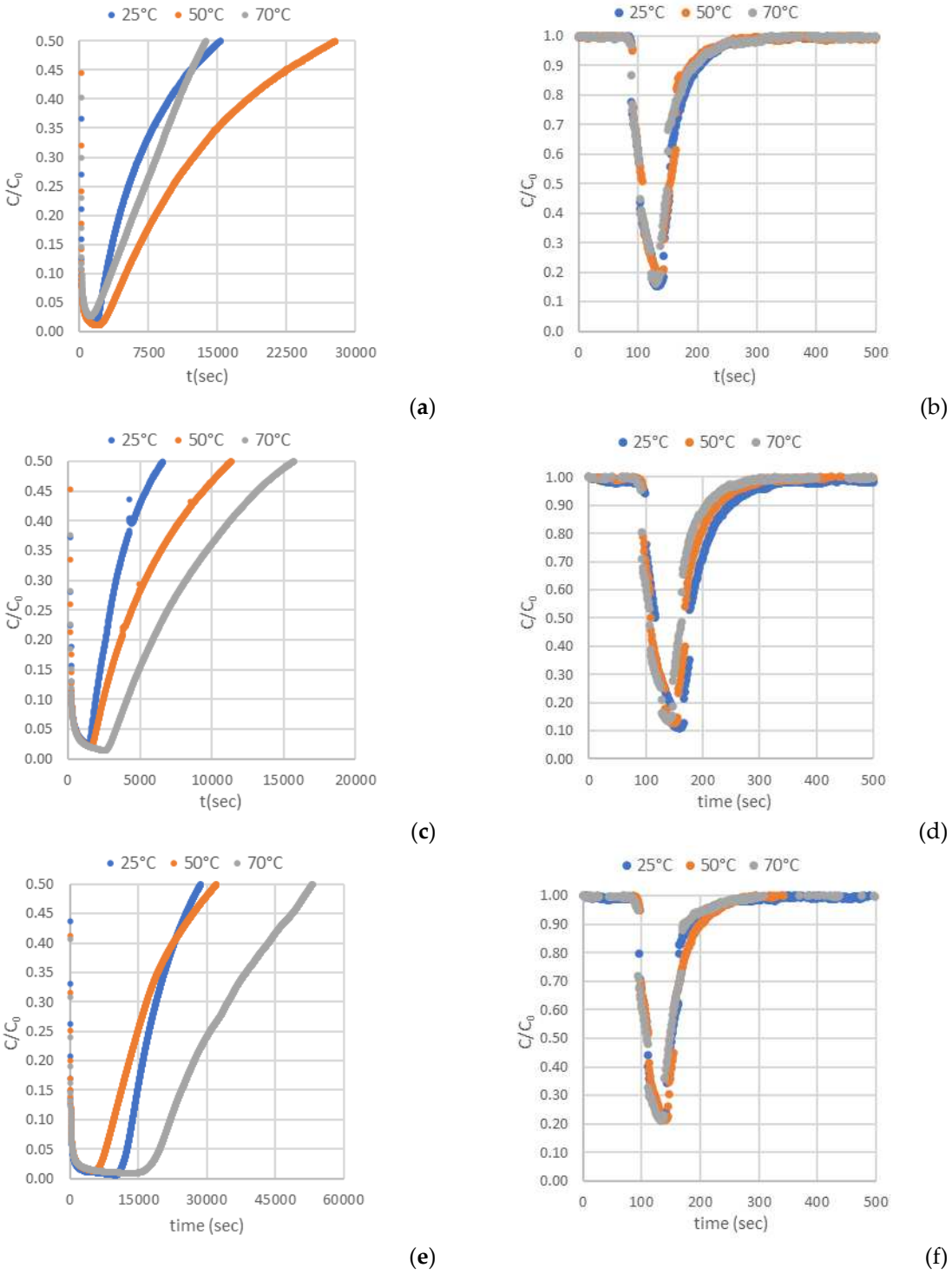

Preprints (www.preprints.org) | NOT PEER-REVIEWED | Posted: 8 June 2023 doi:10.20944/preprints202306.0589.v1

Figure 5. Breakthrough curves of: (a, b) H_2S and CO_2 on AC-H_2O. (c, d) H_2S and CO_2 on AC-KOH. (e, f) H_2S and CO_2 on AC-CO_2.

Table 12. H_2S adsorption capacity, molar mass of H_2S adsorbed per AC mass, on the activated carbon materials in various temperatures.

Activated carbon	Adsorption temperature (°C)	**H_2S capacity (mmol[H_2S]/g)**		
		Breakthrough time (C/C_0=0,05) [1]	Reference time C/C_0=0,5 [1]	Exhaustion time (C/C_0=0,95) [2]
AC-H_2O	25	0.10	0.71	2.13
	50	0.09	1.22	3.26
	70	0.04	0.51	1.54
AC-KOH	25	0.05	0.19	0.88
	50	0.05	0.31	1.42
	70	0.07	0.36	0.79
AC-CO_2	25	0.75	1.83	4.70
	50	0.36	1.82	4.63
	70	0.86	3.50	7.51

[1] Experimental. [2] Calculated.

Table 13. H_2S adsorption capacity, mass of H_2S adsorbed per AC mass, on the activated carbon materials in various temperatures.

Activated carbon	Adsorption temperature (°C)	**H_2S capacity (g[H_2S]/g)**		
		Breakthrough time (C/C_0=0,05) [1]	Reference time C/C_0=0,5 [1]	Exhaustion time (C/C_0=0,95) [2]
AC-H_2O	25	2.79	20.93	62.47
	50	2.70	35.94	95.53
	70	1.20	15.02	45.13
AC-KOH	25	1.46	5.66	25.95
	50	1.40	9.03	41.75
	70	2.12	10.47	23.23
AC-CO_2	25	22.14	53.62	137.83
	50	10.62	53.44	135.65
	70	25.19	102.69	220.17

[1] Experimental. [2] Calculated.

Table 14. CO_2 adsorption capacity, molar mass of CO_2 adsorbed per AC mass, on the activated carbon materials in various temperatures.

Activated carbon	Adsorption temperature (°C)	**CO_2 capacity (mmol[CO_2]/g)**			
		Breakthrough time (C/C_0=0,05) [1]	C/C_0=0,5 [1]	Exhaustion time (C/C_0=0,95) [1]	Reference time C/C_0=0,5 [2]
AC-H_2O	25	0.08	0.19	0.30	0.30
	50	0.00	0.15	0.36	0.36
	70	0.11	0.20	0.38	0.38
AC-KOH	25	0.21	0.62	1.17	1.17
	50	0.13	0.49	0.86	0.86
	70	0.04	0.37	0.54	0.54
AC-CO_2	25	0.07	0.17	0.38	0.38
	50	0.06	0.10	0.10	0.10
	70	0.05	0.11	0.12	0.12

[1] CO_2 breakthrough time, time when C/C_0=0,5 and exhaustion time. [2] Reference time; when C/C_0=0,5 at the adsorption curve of H_2S.

Preprints (www.preprints.org) | NOT PEER-REVIEWED | Posted: 8 June 2023 doi:10.20944/preprints202306.0589.v1

Table 15. CO_2 adsorption capacity, mass of CO_2 adsorbed per AC mass, on the activated carbon materials in various temperatures.

Activated carbon	Adsorption temperature (°C)	CO_2 capacity (g[CO_2]/g)			
		Breakthrough time (C/C₀=0,05) [1]	C/C₀=0,5 [1]	Exhaustion time (C/C₀=0,95) [1]	Reference time C/C₀=0,5 [2]
AC-H_2O	25	1.82	4.32	6.82	6.82
	50	0.00	3.41	8.18	8.18
	70	2.50	4.54	8.63	8.63
AC-KOH	25	4.77	14.09	26.58	26.58
	50	2.95	11.13	19.54	19.54
	70	0.91	8.41	12.27	12.27
AC-CO_2	25	1.59	3.86	8.63	8.63
	50	1.36	2.27	2.27	2.27
	70	1.14	2.50	2.73	2.73

[1] CO_2 breakthrough time, time when C/C₀=0,5 and exhaustion time. [2] Reference time; when C/C₀=0,5 at the adsorption curve of H_2S.

Table 16. Selectivity of H_2S over CO_2 on the activated carbon materials in various temperatures.

Activated carbon	Reactor temperature (°C)	Selectivity of H_2S		
		Breakthrough time (C/C₀=0,05) [1]	Reference time C/C₀=0,5 [1]	Exhaustion time (C/C₀=0,95) [2]
AC-H_2O	25	254	1903	5680
	50	204	2719	7227
	70	86	1081	3248
AC-KOH	25	34	132	606
	50	45	288	1331
	70	106	525	1166
AC-CO_2	25	1573	3810	9795
	50	2902	14606	37075
	70	5607	22859	49010

[1] Experimental. [2] Calculated.

The results clearly show that the carbons derived from the physical activation of biochar exhibit higher adsorption capacity for H_2S and lower CO_2 adsorptivity as compared to the sample produced by the chemical activation method with KOH. A distinguishing feature of these samples is that despite their moderate BET surface and micropore volume, they hold a quite extended mesopore structure with a PSD centered around 50Å. In addition, contrarily to what happens with the AC-KOH sample, the mesopores of the physically activated carbons preserve a high population of surface oxygenated functional groups. Hence it becomes evident that H_2S is strongly hindered from entering the micropore structure of ACs and is mostly adsorbed in the mesopores, benefited also by its strong interaction with the functional groups. On the other hand, micropores are fully accessible for CO_2 and this explains the much higher CO_2 adsorptivity of AC-KOH as compared to AC-H_2O and AC-CO_2. Supporting to these statements is that between the two physically activated samples, AC-CO_2, despite its lower BET surface, is a more effective adsorbent for H_2S because of its more extended mesopore structure (see Table 11) and possibly due to the higher population of oxygenated functional groups (Figure 4). Regarding the effect of temperature, in the case of H_2S a maximum of the adsorptivity is observed systematically for all samples at 50 °C or a continuous increase up to 70 °C, something that doesn't happen with CO_2 which in most of the experiments follows the normal trend of the adsorption exotherm. The maximum in the H_2S adsorptivity with the temperature comes as a result of the counterbalance between adsorption and diffusion. This unveils that due to the strongly acidic character of H_2S, its adsorptivity is controlled by diffusion, meaning that when the H_2S

molecules enter the pore, they reside long period on an adsorption site before hopping to the next unsaturated one. Diffusion is an activated process and is fortified as the temperature increases, whereas adsorption is attenuated, and this counterbalance generates the maximum observed in our experiments.

4. Conclusions

This work concludes that in order to achieve the production of effective activated carbon adsorbents from the solid fibrous digestate (SFD) of biogas plants, washing with HNO_3 to remove the inorganic content and expand the carbonaceous yield is a mandatory pre-treatment process. Moreover, biochar intermediate can be produced by pyrolysis at moderate temperatures up to 600^{o}C with no effect on the quality of the subsequently derived ACs, which is of high importance for the sustainability of the proposed methodology. Notably, simple chemical and physical activation processes of the produced biochars conclude to very effective CO_2 and H_2S adsorbents respectively, paving the way for the achievement of a closed loop value chain where the waste effluent of a biogas plant is transformed to effective adsorbents that can be used in series to desulphurise and upgrade biogas.

Author Contributions: Conceptualization, G.R., E.K. and T.S.; methodology, G.R., A.L., S.S., and E.K.; software, G.R.; validation, G.R., E.K., A.L. and T.S.; formal analysis, G.P. and G.D.; investigation, A.M. and G.D.; resources, A.M.; data curation, E.C., S.S., G.P.; writing—original draft preparation, E.C., G.R.; writing—review and editing, G.R., T.S. and E.C.; visualization, E.C.; supervision, G.R.; project administration, T.S.; funding acquisition, T.S. All authors have read and agreed to the published version of the manuscript.

Funding: This research was co-funded by the European Regional Development Fund of the Eu- European Union and Greek national funds through the Operational Program Competitiveness, Entrepreneurship and Innovation, under the call RESEARCH – CREATE – INNOVATE (project code: T2EDK-00455 PYRO-D).

Institutional Review Board Statement: Not applicable.

Informed Consent Statement: Not applicable.

Data Availability Statement: The data presented in this study are available upon request from the corresponding author.

Acknowledgments: The authors acknowledge all staff members of Qlab P.C. and NCSR "Democritus" for their individual roles that contributed to the implementation of this study.

Conflicts of Interest: The authors declare no conflict of interest.

References

1. McKinsey, S. Z. Removal of Hydrogen Sulfide from Biogas using cow-manure compost. A Thesis Faculty of the Graduate School of Cornell University, **2003**.
2. Kulkarni, M.B.; Ghanegaonkar, P.M. Hydrogen sulfide removal from biogas using chemical absorption technique in packed column reactors. *Global Journal of Environmental Science and Management* **2019**, 5(1), pp.155-166.
3. Shareefdeen; Z., Singh; A. Biotechnology for odor and air pollution control, **2005**.
4. Weiland, P. Notwendigkeit der Biogasaufbereitung, Ansprüche einzelner Nutzungsrouten und Stand der Technik.
5. Allegue, L.B.; Hinge, J. Biogas upgrading Evaluation of methods for H_2S removal, Danish Technological Institute, **2014**, https://www.teknologisk.dk/_/media/60599_Biogas%20upgrading.%20Evaluation%20of%20methods%20for%20H2S%20removal.pdf
6. Xiao-fei, T.; Shao-bo, L.; Yun-guo, L.; Yan-ling, G.; Guang-ming. Z.; Xin-jiang, H.; Xin, W.; Shao-heng, L.; Lu-hua, J. Biochar as potential sustainable precursors for activated carbon production: Multiple applications in environmental protection and energy storage. *Bioresource Technology* **2017**, *227*, pp.359-372.
7. Georgiadis, A.G.; Charisiou, N.D.; Goula, M.A. Removal of hydrogen sulfide from various industrial gases: A Review of the most promising adsorbing materials. *Catalysts* **2020**, *10(5)*, pp.521; https://doi.org/10.3390/catal10050521

8. Guo, J.; Luo, Y.; Chong Lua, A.; Chi, R.; Chen Y.; Bao, X.; Xiang, S. Adsorption of hydrogen sulphide (H_2S) by activated carbons derived from oil-palm shell. *Carbon* **2007**, *45*, pp.330–336.
9. Pallarés, J.; González-Cencerrado, A.; Arauzo, I. Production and characterization of activated carbon from barley straw by physical activation with carbon dioxide and steam. *Biomass and Bioenergy* **2018**, *115*, pp.64-73.
10. Chiung-Fen, C.; Ching-Yuan, C.; Wen-Tien, T. Effects of Burn-off and Activation Temperature on Preparation of Activated Carbon from Corn Cob Agrowaste by CO_2 and Steam. *Journal of Colloid and Interface Science* **2000**, *232 (1)*, pp. 45-49.
11. Farma, R.; Deraman, M.; Awitdrus, A.; Talib, I.A.; Taer, E.; Basri, N.H.; Manjunatha, J.G.; Ishak, M.M.; Dollah, B.N.M.; Hashmi, S.A. Preparation of highly porous binderless activated carbon electrodes from fibres of oil palm empty fruit bunches for application in supercapacitors. *Bioresource Technology* **2013**, *132*, pp.254-261.
12. Molina-Sabio, M.; Gonzalez, M.T.; Rodriguez-Reinoso, F.; Sepúlveda-Escribano, A. Effect of steam and carbon dioxide activation in the micropore size distribution of activated carbon. *Carbon* **1996**, *34 (4)*, pp.505-509
13. Hussain, A. A computational study of adsorption of H_2S and SO_2 on the activated carbon surfaces. *Journal of Molecular Graphics and Modelling* **2023**, *122*, 108463.
14. Plaza, M.G.; González, A.S.; Pis, J.J.; Rubiera, F.; Pevida, C. Production of microporous biochars by single-step oxidation: Effect of activation conditions on CO_2 capture. *Applied Energy*, **2014,** *114*, pp.551-562
15. Aworn, A.; Thiravetyan, P.; Nakbanpote, W. Preparation and characteristics of agricultural waste activated carbon by physical activation having micro- and mesopores. *Journal of Analytical and Applied Pyrolysis* **2008**, *82 (2)*, pp.279-285
16. Kainourgiakis, M.E.; Steriotis, Th.A.; Kikkinides; E.S.; Romanos, G.; Stubos, A.K. Adsorption and diffusion in nanoporous materials from stochastic and process-based reconstruction techniques. *Colloids and Surfaces A: Physicochemical and Engineering Aspects* **2002**, *206 (1–3)*, pp. 321-334.
17. Romanos, G.E.; Vangeli, O.C.; Stefanopoulos, K.L.; Kouvelos, E.P.; Papageorgiou, S.K.; Favvas, E.P.; Kanellopoulos, N.K. Methods of evaluating pore morphology in hybrid organic–inorganic porous materials. *Microporous and Mesoporous Materials* **2009**, *120 (1–2)*, pp. 53-61
18. Pokhrel, J.; Bhoria, N.; a, Anastasiou, S.; Tsoufis, T.; b, Gournis, D.; Romanos, G.; Karanikolos, G.N. CO_2 adsorption behavior of amine-functionalized ZIF-8, graphene oxide, and ZIF-8/graphene oxide composites under dry and wet conditions. *Microporous and Mesoporous Materials* **2018**, *267*, pp. 53-67
19. Aik Chong, L.; Fong Yow, L.; Jia, G. Influence of pyrolysis conditions on pore development of oil-palm-shell activated carbons. Journal of Analytical and Applied Pyrolysis **2006**, *76 (1-2)*, pp.96-102.
20. Bouchelta, C.; Medjram, M.S.; Zoubida, M.; Chekkat, F.A.; Ramdane, N.; Bellat, J. Effects of pyrolysis conditions on the porous structure development of date pits activated carbon. *Journal of Analytical and Applied Pyrolysis* **2012**, *94*, pp.215-222
21. Stefanidis, S.D.; Kalogiannis, K.G.; Iliopoulou, E.F.; Michailof, C.M.; Pilavachi, P.A.; Lappas, A.A. A study of lignocellulosic biomass pyrolysis via the pyrolysis of cellulose, hemicellulose and lignin. *Journal of Analytical and Applied Pyrolysis* **2014**, *105*, pp.143-150
22. Antonakou, E.V.; Kalogiannis, K.G.; Stefanidis, S.D.; Karakoulia, S.A.; Triantafyllidis, K.S.; Lappas, A.A.; Achilias, D.S. Catalytic and thermal pyrolysis of polycarbonate in a fixed-bed reactor: The effect of catalysts on products yields and composition. *Polymer Degradation and Stability* **2014**, *110*, pp. 482-491